Desalination and Water Treatment
www.deswater.com

doi: 10.5004/dwt.2020.26065

201 (2020) 420–430
October

Photocatalytic degradation of congo red by using PANI and PANI/ZrO_2: under UV-A light irradiation and dark environment

Sibel Zor*, Bilge Budak

Department of Chemistry, Kocaeli University Science – Art Faculty, Kocaeli, Turkey, Tel. +90 262 303 2034; Fax: + 90 292 303 2003; email: merve@kocaeli.edu.tr (S. Zor), Tel. +90 262 303 2022; email: bilgebudak.bb@gmail.com (B. Budak)

Received 17 December 2019; Accepted 2 May 2020

ABSTRACT

In this study, polyaniline (PANI) and polyaniline nanometal oxide (PANI/ZrO_2) composites synthesized by the chemical polymerization method were structurally characterized by X-ray diffraction, Fourier-transform infrared spectroscopy, scanning electron microscopy, and transmission electron microscopy methods. The thermal behavior of polymeric composites was analyzed using thermogravimetric analysis. Bandgap energy of PANI and PANI/ZrO_2 were calculated by using the Tauc plot. The photocatalytic effect of PANI nanocomposites with and without nano-ZrO_2 in different amounts (0.1, 0.5, and 1.0 wt.%) on the degradation of congo red dye was investigated under UV-visible light irradiation (UV-A, 365 nm) and a dark environment. The effect of light on 100% of the degradation of the congo red was investigated by using PANI and PANI/ZrO_2 photocatalysts. PANI and PANI/ZrO_2 catalysts under UV-A light irradiation were found to be more effective in 100% the degradation of the congo red dye molecules than that of in the dark environment. The photocatalytic activities of the catalysts were increased by the addition of nano-ZrO_2 to the PANI structure. The reaction kinetics were investigated by using the first-order reaction kinetic model. The photocatalytic reaction rate was higher by increasing the amount of nano-ZrO_2 used in the polymeric composite.

Keywords: PANI; PANI/ZrO_2; Congo red; Photocatalytic degradation; Wastewater

1. Introduction

Industrial wastewater is one of the most important sources of pollution in surface and groundwater. Wastewater is treated in the treatment plants and then released to the environment. However, it should be noted that reactive dyes cannot be removed by a regular treatment process and the water from the wastewater plant contains reactive dyes despite the removal process. Unfortunately releasing water containing reactive dyes into the environment let to remain dye compounds in the environment for many years without degradation. These reactive dyes are very toxic to human health are the leading causes of cancer diseases [1,2]. One of the environmentally harmful dyes is congo red (CR), which is the sodium salt of the acid called benzidine diazo-bis-1-naphthylamine-4-sulfonic acid. Although CR has carcinogenic and mutagenic properties, it is widely used in the textile, paper, printing, and plastic industries [3,4].

Various physical and chemical methods such as ion exchange, electrochemical and photochemical decomposition, reverse osmosis, ultrafiltration adsorption, and chemical oxidation could be used for removal of dyes from wastewater [5–8]. Although chemical flocculation and sedimentation are some of the common methods used to remove dye materials from wastewater, it is harmful due to the chemical contaminants formed. Due to the complex organic structure of the dyes and their ability to withstand biological degradation, biological methods are insufficient in color removal [9]. For this reason, photocatalytic degradation, which is known to be environmentally friendly, has become

* Corresponding author.

an important method. When exposed to UV light, the photocatalysts used in photocatalytic degradation become highly energized by absorbing light. It initiates the chemical reaction by transferring the reactive material around this energy. The resulting high oxidation oxidizes the harmful substances in contact with the power by converting them into CO_2, H_2O, and other small molecules. Photocatalytic processes are also widely used in different applications such as self-cleaning of materials, deodorization, and water treatment [10,11].

Photocatalysis is the process in which light and catalyst are combined together to initiate or accelerate a chemical reaction. Briefly, photocatalysis can be defined as the catalyzed acceleration of a light-induced reaction [12]. The use of composites obtained by modification of conductive polymers and semiconductor metal oxides in dye removal by photocatalytic degradation is one of the popular research topics [13–19]. Many types of semiconducting systems have been studied for photocatalysis including TiO_2, ZnO, ZrO_2, CdS, WO_3, and so on [20–23]. Most of them have a bandgap in the UV (ultraviolet) region, that is, equal to or greater than 3.36 eV (λ = 388 nm) Thus, these catalysts promote photocatalytic reactions under the illumination of UV radiation [24]. One of these semiconductors, ZrO_2, is considered as a photocatalyst in different chemical reactions due to the high negative value of the broad bandgap and the conduction band potential. The bandgap energy of ZrO_2 is 5.1 eV [25]. ZrO_2 nanoparticles are effective antibacterial and anticorrosion agents with many properties such as high strength, abrasion resistance, fracture toughness, hardness, and chemical resistance [26,27].

Semiconductors are effective under UV light irradiation when used as photocatalyst alone. To increase the efficiency of semiconductors under visible light irradiation, polymeric composite is formed with conductive polymers. The most widely used conductive polymer for this purpose is polyaniline [28,29].

In this study, PANI and PANI/ZrO_2 nanocomposites were synthesized by chemical polymerization and these nanocomposites were characterized by X-ray diffraction (XRD), Fourier-transform infrared spectroscopy (FTIR), scanning electron microscopy (SEM) and transmission electron microscopy (TEM) methods. The thermal analysis of polymeric nanocomposites was performed by thermogravimetric analysis (TGA). Also, the bandgap energy of photocatalysts was determined by drawing the Tauc plot. The photocatalytic effect on the degradation of the CR of PANI, PANI/ZrO_2 photocatalysts was examined under the UV-A light irradiation and a dark environment.

2. Experimental

2.1. Materials and methods

ZrO_2 nanoparticles (<100 nanoparticle size, CAS: 1314-23-4, Mw = 123.22 g/mol), 37% hydrochloric acid (HCl), 99.5% aniline (ANI, C_6H_7N), ammonium peroxydisulfate (APS, $(NH_4)_2S_20_8$), sodium chloride (NaCl), ethanol (C_2H_6O). Congo red dye (CR, $C_{32}H_{22}N_6Na_2O_6S_2$), coloring agent, CI 22120, BDH Chemical Ltd., UK. All other chemicals are supplied by Merck. The chemical substances were used without purification.

2.2. Synthesis of PANI and PANI/ZrO_2 nanocomposites

Synthesis of PANI; 1 mL of aniline was added to the 70 mL 2.0 M HCl solution. The solution was stirred with a magnetic stirrer at a constant speed. To this was added by dropwise a solution of 2.5 g of APS in 20 ml of deionized water. Polymerization continued at room temperature for about 5 h. The crude product was filtered and washed with 2 M HCl solution, ethyl alcohol, and deionized water. The resulting solid product was dried at 60°C under vacuum.

Synthesis of the PANI/ZrO_2 polymeric nanocomposite is similar to the synthesis of the PANI, and the same procedure was performed with the addition of ZrO_2 (0.1, 0.5, and 1.0 wt.%) metal oxide nanoparticles. ZrO_2 metal oxide nanoparticles were added into the 70 mL of 2.0 M HCl solution, then 1 mL of aniline was added while the prepared solution was stirring. The resulting solution was stirred with a magnetic stirrer at constant speed 1 h and then kept for 1 h in an ultrasonic bath (to provide dispersion of nanoparticles). After adding APS solution (2.5 g of APS in 20 ml of deionized water), the procedures were repeated while preparing the pure PANI.

2.3. Photodegradation experiments

The photocatalytic degradation of the CR dye was carried out using the PANI and PANI/ZrO_2 photocatalysts under UV visible light (365 nm, UV-A) irradiation. A high-pressure sodium lamp (OSRAM, VIALOX SON-T, 400 W, Germany) that radiates predominately between 400 and 700 nm wavelengths was used in the tests. The maximum wavelength (λ_{max}) for CR was found to be 499–500 nm [30]. Photocatalytic experiments were carried out at room temperature. In photocatalytic experiments, a UV photo booth with UV lamp pair containing 254 nm short wave and 365 nm long wavelength was used as a light source. During the photocatalytic degradation experiments of the CR dye, a 365 nm wavelength lamp in the UV cabinet was used.

Photocatalytic degradation of CR under UV-A light irradiation was performed using a UV cabinet at 365 nm wavelength. The dye solution at a concentration of 100 mg/L was prepared in deionized water and 0.1 g amounts of PANI and PANI/ZrO_2 nanocomposites as photocatalyst were added into 100 mL dye solution and the mixture was stirred at dark medium for desired times to equilibrate. Concentration and wavelength measurements were made by taking samples from the solution at certain time intervals with a spectrophotometer. Degradation was repeated with and without light for each solution.

The lamp was switched on to initiate the photocatalytic degradation reaction. During irradiation, the suspension was stirred continuously to keep the suspension homogeneous. Concentrations of the dye solution were measured using a UV spectrophotometer, after centrifugation of the degraded dye solution.

The photocatalytic degradation experiments of the dye were continued until 100% of degradation occurred at specific time intervals. The same experiments were repeated in the dark medium. The degradation % was calculated using the following equation [31]:

$$\text{Degradation \%} = \left(\frac{(C_0 - C)}{C_0} \right) \times 100 \quad (1)$$

where C_0, is the initial concentration of the dye and C is the concentration of the dye after UV-A light irradiation.

A calibration curve was plotted by reading the absorbance values of samples with known concentrations. The calibration curve was used to determine the concentrations of the samples. The concentrations of the solutions to be used in the calibration chart was determined to conform to the Lambert–Beer law [32,33].

2.4. Characterization methods

TGA of PANI and PANI/ZrO_2 polymeric nanocomposites synthesized by the chemical polymerization method was performed with the Mettler Toledo analyzer (heating rate 10°C/min). XRD measurements of the samples were made with a Bruker Advanced D8 XRD instrument. SEM analysis of the samples was determined using Cressington 208 C (Electron Microscopy Center, North Dakota University) and TEM analysis using the JEOL-2100 LaB6 device (Electron Microscopy Center, North Dakota University) for the determination of the morphological and structural properties of the nanocomposites. FTIR spectra of powdered PANI and PANI/ZrO_2 nanocomposites were recorded using a Perkin-Elmer-2000 infrared spectrophotometer (KBr reference sample) series at 4,000–600 cm^{-1} wave number. Photocatalytic activity measurements were also made using a Perkin-Elmer UV Lambda 25 spectrophotometer (Kocaeli University, Chem. Lab.).

3. Results and discussions

3.1. FTIR analysis

The FTIR spectral curves of PANI and PANI/ZrO_2 (0.1, 0.5, and 1.0 wt.% nano-ZrO_2) nanocomposites are shown in Fig. 1. Characteristic absorption peaks of polymeric nanocomposites are presented in Table 1. The characteristic peaks of PANI, N–H stretching mode at 3,455 cm^{-1}, C=C stretching of benzenoid rings at 1,494 cm^{-1}, planar vibration of C–H bond at 1,109 cm^{-1}, stretching of C–N benzene rings at 1,291 cm^{-1}, the stretching of the C=N quinoid rings at 1,583 cm^{-1} and the stretching of the C–C aromatic rings at 797 cm^{-1} [34] were detected. The values obtained are consistent with the literature [35] when the absorption spectra of nanoparticle-containing polymeric composites are compared with PANI, there is a shift due to the unique interactions between PANI and ZrO_2 nanoparticles [28] (Table 1). as listed in Table 1, the N–H stretching in PANI is 3,455 cm^{-1} and 3,446 cm^{-1} in PANI/ZrO_2 (0.1 wt.%), 3,422 cm^{-1} in PANI/ZrO_2 (0.5 wt.%) and 3,380 cm^{-1} in PANI/ZrO_2 (1.0 wt.%). Another example of this shift is the shifts in the C–N stretching mode of benzenoid rings, the C–N stretching mode of benzenoid rings for PANI is 1,291 and 1,255 cm^{-1} for PANI/ZrO_2 (0.1 wt.%), 1,253 cm^{-1} for PANI/ZrO_2 (0.5 wt.%) and 1,250 cm^{-1} for PANI/ZrO_2 (1.0 wt.%). were determined. Peaks from 3,050 to 3,500 cm^{-1} indicating the cross-linking mode of the polymer chains. The addition of ZrO_2 to PANI is attributed to Zr–O stretching and shows the presence of metal oxides at 500–600 cm^{-1}. This peak is clearly seen in the FTIR spectrum of the polymeric composite containing 1.0 wt.% ZrO_2 [28,36].

3.2. TGA results

TGA results of PANI and PANI/ZrO_2 (0.1, 0.5, and 1.0 wt.%) nanocomposites are shown in Fig. 2. There are three stages of weight loss of nanocomposites containing different amounts of ZrO_2. PANI, an organic polymer, is not very stable when heated and its initial weight loss is in the range of 100°C–200°C, which is associated with the evaporation of water molecules in the structure of the polymers [37]. Due to the melting or evaporation of PANI, a second weight loss occurred at 240°C and 250°C. Finally, due to the thermal decomposition of the polymeric chains, a third weight loss occurs at a high temperature of about 550°C–600°C [38].

The total weight loss for PANI was about 98%–99%, the weight loss for PANI/ZrO_2 (0.1 wt.%) was 30%, for PANI/ZrO_2 (0.5 wt.%) was 22%, and for the PANI/ZrO_2 (1.0 wt.%) was about 19%. By incorporating ZrO_2 into the polymeric network structure, the reduction in weight loss indicates that the thermal stability of the polymeric nanocomposite is increased [39].

3.3. SEM and TEM results

SEM photographs of the synthesized polymeric nanocomposites are given in Fig. 3. PANI appears to be in a spherical structure. With the addition of ZrO_2 in polymeric composites, the metal oxide particles in the form of rod-like structure enter between the PANI molecules, and in some regions, the ZrO_2 molecules in the nanostructures come together to form agglomerates (Figs. 3a–d). On the polymeric surface, ZrO_2 nanoparticles formed a helical structure.

Table 1
FTIR spectra of PANI and PANI/ZrO_2 polymeric nanocomposites

Type of nanocomposite	N–H stretching mode (cm^{-1})	C=C stretching mode of benzenoid rings (cm^{-1})	C–H and C=C stretching mode of aromatic rings (cm^{-1})	C–N stretching mode of benzenoid rings (cm^{-1})	C=N stretching mode of quinoid rings (cm^{-1})	Plane bending vibration of C–H bonds (cm^{-1})
PANI	3,455	1,494	1,109	1,291	1,583	797
PANI/ZrO_2 (0.1 wt.%)	3,446	1,450	1,110	1,255	1,712	654
PANI/ZrO_2 (0.5 wt.%)	3,422	1,438	1,108	1,253	1,723	651
PANI/ZrO_2 (1.0 wt.%)	3,380	1,435	1,115	1,250	1,734	647

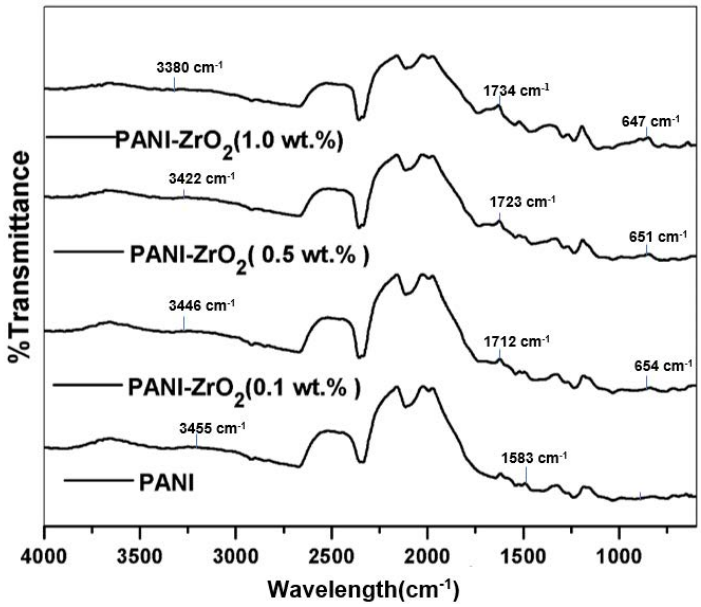

Fig. 1. FTIR spectra of PANI and PANI/ZrO_2 polymeric nanocomposites.

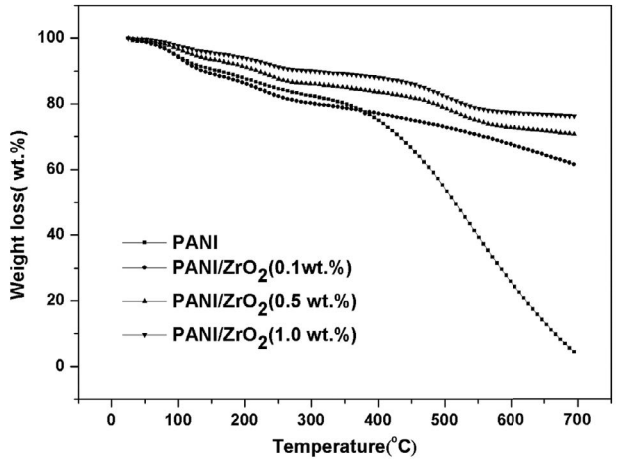

Fig. 2. TGA curves of PANI and PANI/ZrO_2 nanocomposites.

The PANI/ZrO_2 nanocomposite synthesized by the chemical polymerization method exhibits rod-like structures [40].

TEM images of PANI and PANI/ZrO_2 are shown in Fig. 4. In the TEM images of the PANI, the cloudy network structure is evident (Fig. 4a). It is seen that PANI is incorporated into the polymeric matrix by the addition of ZrO_2 nanoparticles, nano ZrO_2 molecules are present in the polymeric matrix and agglomerated in some regions (Figs. 4a–d). TEM images of different amounts of catalysts contain small dark spots that can result from Zr-rich domains [41]. SEM and TEM results support each other.

3.4. XRD patterns

XRD patterns of synthesized nanoparticles by the chemical polymerization method are given in Fig. 5. As shown in Fig. 5, 4 characteristic peaks at 2θ angle for PANI; 14.786°, 20.022°, 24.861°, 35.434°. Also, Pouget et al. [43] found that 2θ for the PANI polymer was 20.3° and 25.1°. Generally, polymers can be expected to be amorphous in structure, however, the synthesized PANI polymers are obtained as crystalline due to the planar nature of the benzenoid and quinoid functional groups [42]. When PANI is encapsulated with the ZrO_2 nanoparticle, the interaction of PANI and ZrO_2 restricts the growth of the PANI chains around the ZrO_2 nanoparticles. The crystallinity behavior of PANI is inhibited and the degree of crystallinity is reduced [43]. There is a marked shift in the peaks of nanocomposites prepared by adding ZrO_2 in the XRD models of PANI/ZrO_2 nanoparticles. With the increase of the added ZrO_2 metal oxide fraction, the shift is further increased. The characteristic peaks of the PANI/ZrO_2 nanocomposite at 2θ angle are as follows; 17.505°, 24.034°, 35.339°, 44.792°, and 50.124°, respectively (Fig. 5). The XRD results obtained are consistent with the literature data [44].

3.5. UV-visible spectra and bandgap energy

The UV-visible absorption spectra of photocatalysts were analyzed to investigate the effect of PANI and ZrO_2 nanoparticles on spectroscopic absorption of ZrO_2 nanoparticles. The UV-visible spectrum of ZrO_2 nanoparticles, PANI and PANI/ZrO_2 nanocomposites are given in Fig. 6. For use in the measurement of UV-visible absorption spectroscopy, the powdered PANI was dissolved in methanol, PANI/ZrO_2 and ZrO_2 were dissolved in nitric acid. Spectra of all samples were recorded at room temperature using a spectrophotometer in the wavelength range from 200 to 700 nm.

The PANI shows a sharp absorption band at ~240 nm which is due to π–π* electron transition (from HOMO to LUMO). The π–π* electronic transition is associated with the extent of conjugation between the phenylene rings in

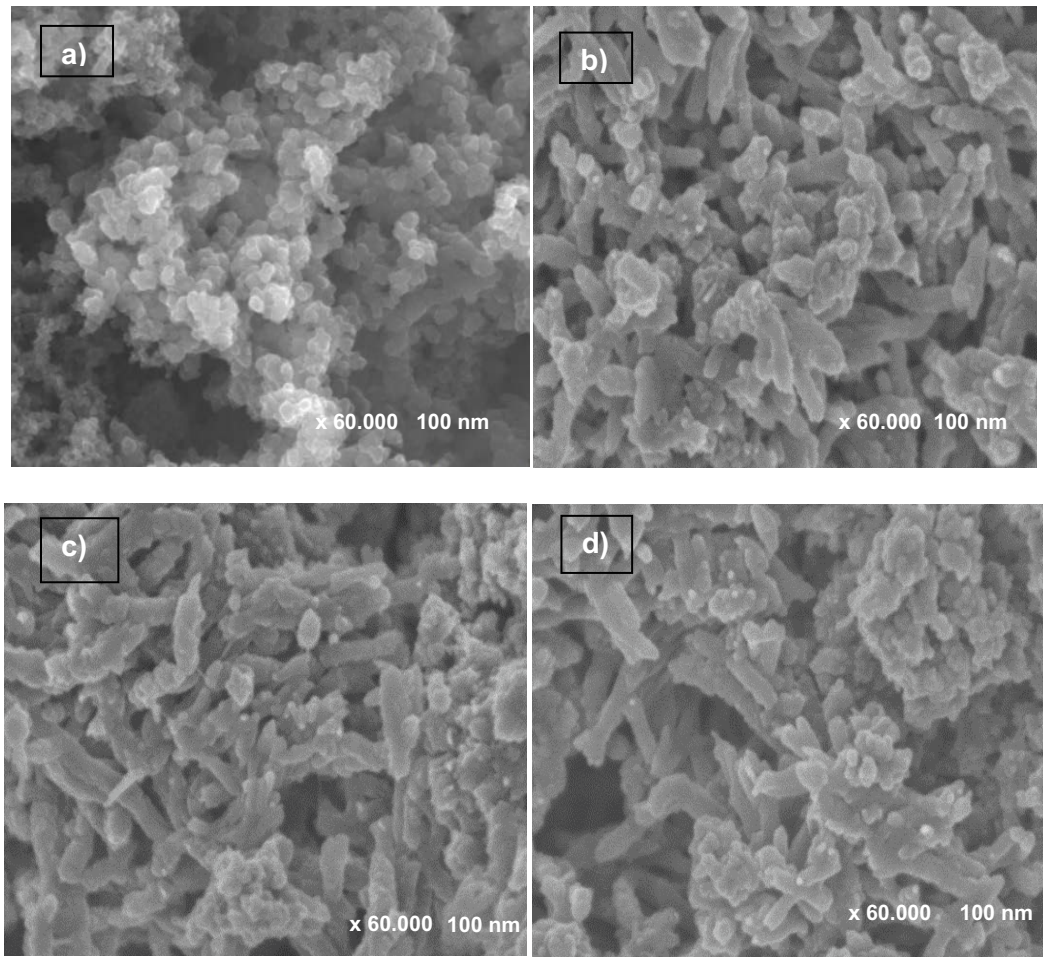

Fig. 3. SEM images for (a) PANI, (b) PANI/ZrO_2 (0.1 wt.%), (c) PANI/ZrO_2 (0.5 wt.%), and (d) PANI/ZrO_2 (1.0 wt.%).

the polymeric chain and π-system. This association lowers the bandgap due to the augmentation of conjugation [45]. It is the π–π* transition of the benzenoid ring and the formation of the polaron band which is solely responsible for the large increase of the electrical conductivity of the nanocomposites [46,47]. The broad absorption band around ~390 nm arises due to polaron–π* transition indicating the protonic nature of polyaniline. In the absorption spectrum of ZrO_2, two sharp peaks are observed at a wavelength of approximately 232.5 nm and a wavelength of 370 nm. The observed peak at the wavelength of 232.5 nm is associated with the bandgap of ZrO_2 (5.3 eV), while the peak at 370 nm is due to the transition between the bands. The peaks observed in PANI and ZrO_2 are also seen in the PANI/ZrO_2 absorption spectrum [48,49].

Bandgap energy is important in the photocatalytic activity of semiconductor metal oxides. This can be experimentally calculated from Tauc plot using the UV-visible data [50,51],

$$\alpha h\nu = A\left(h\nu - E_g\right)^n \tag{2}$$

where α is the absorption coefficient (cm^{-1}), h is Planck's constant (Js), ν is the frequency of radiation (Hz), A is an appropriate constant, E_g is the optical band gap (eV) and n is a constant. The indicates n attained different values such as 1/2, 3/2, 2, 3 depending on the type of transitions like direct allowed or forbidden or indirect allowed or forbidden transitions [52]. Since an allowed indirect transition is considered for ZrO_2 and PANI/ZrO_2, $n = 2$ for our estimations.

The Tauc plot of photon energy ($h\nu$) vs. $(\alpha h\nu)^2$ is shown in Fig. 7.

As shown in Fig. 7, the curved intersection in the photon energy axis, that is, backward extrapolation, gives the bandgap energy of the samples. The bandgap energy of ZrO_2 (a) is 4.9 eV and PANI/ZrO_2 (b) 3.25 eV and the bandgap energy of PANI/ZrO_2 is decreased to 3.25 eV by adding PANI as shown in Fig. 7 [52].

3.6. Photocatalytic activity results

The effect of 0.1 g PANI photocatalysts with and without different amounts of nano-ZrO_2 on the photocatalytic degradation of 100 ppm CR under UV-A irradiation and in the dark environment was investigated. For this purpose, a change of degradation % (at Eq. 1) of the dye with time under UV-A light irradiation and darkness is given in Fig. 8. According to the degradation %-t (min) graph, the degradation rate of 100 ppm CR is quite high under UV light irradiation. Also, the increase in ZrO_2 nanoparticles

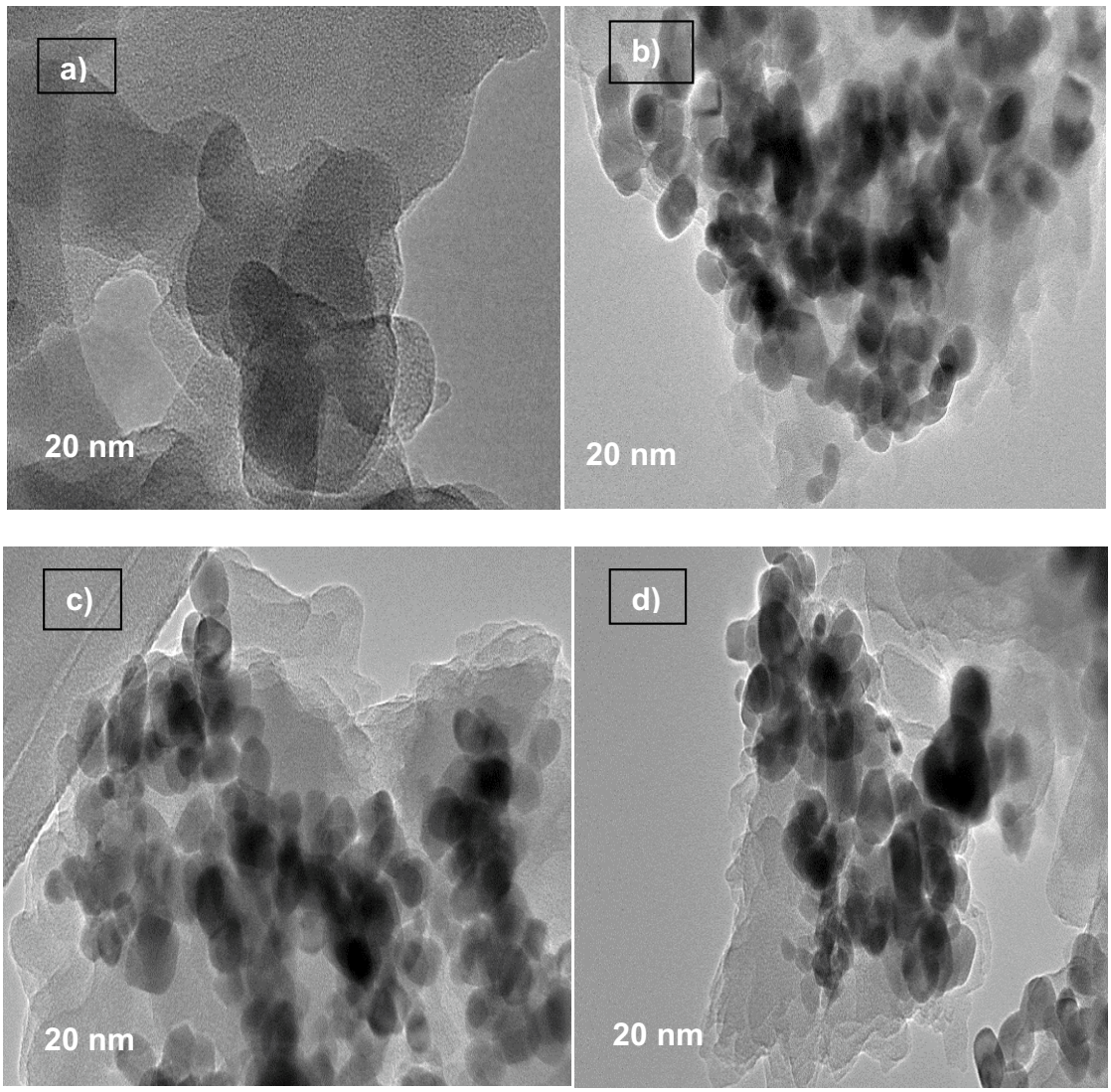

Fig. 4. TEM images for (a) PANI, (b) PANI/ZrO_2 (0.1 wt.%), (c) PANI/ZrO_2 (0.5 wt.%), and (d) PANI/ZrO_2 (1.0 wt.%).

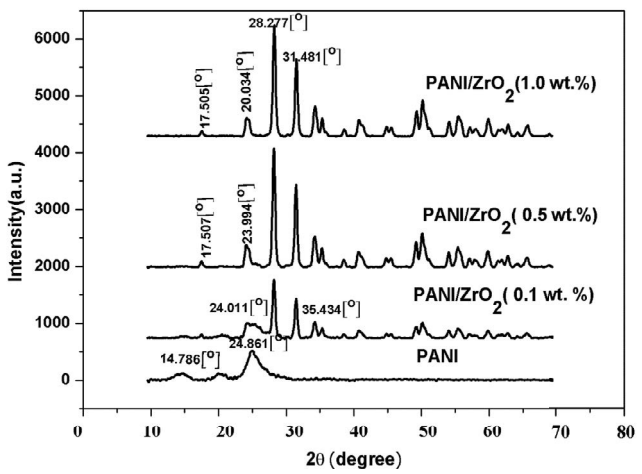

Fig. 5. XRD patterns of PANI and PANI/ZrO_2 polymeric nanocomposites.

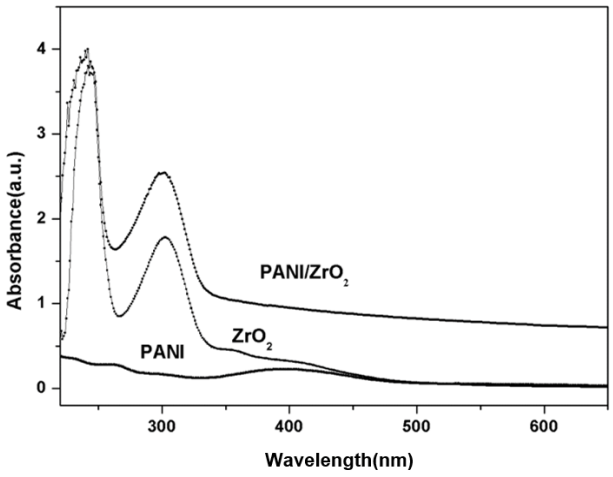

Fig. 6. UV-visible spectrum curves of ZrO_2 nanoparticles, PANI, and PANI/ZrO_2 nanocomposites.

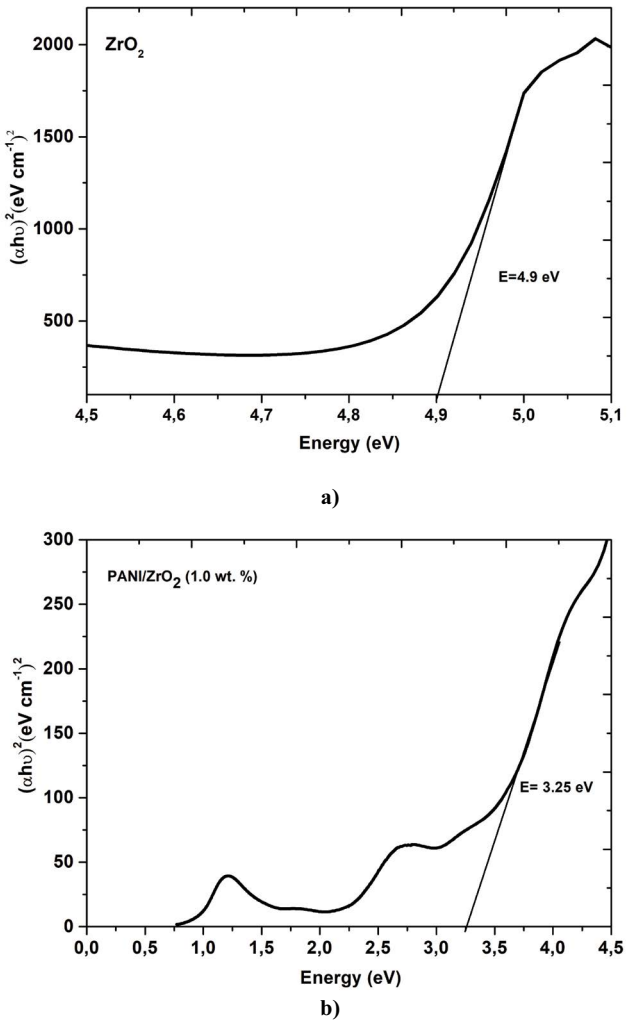

Fig. 7. Tauc plots and bandgap energies of (a) ZrO_2 and (b) PANI/ZrO_2 (1.0 wt.%).

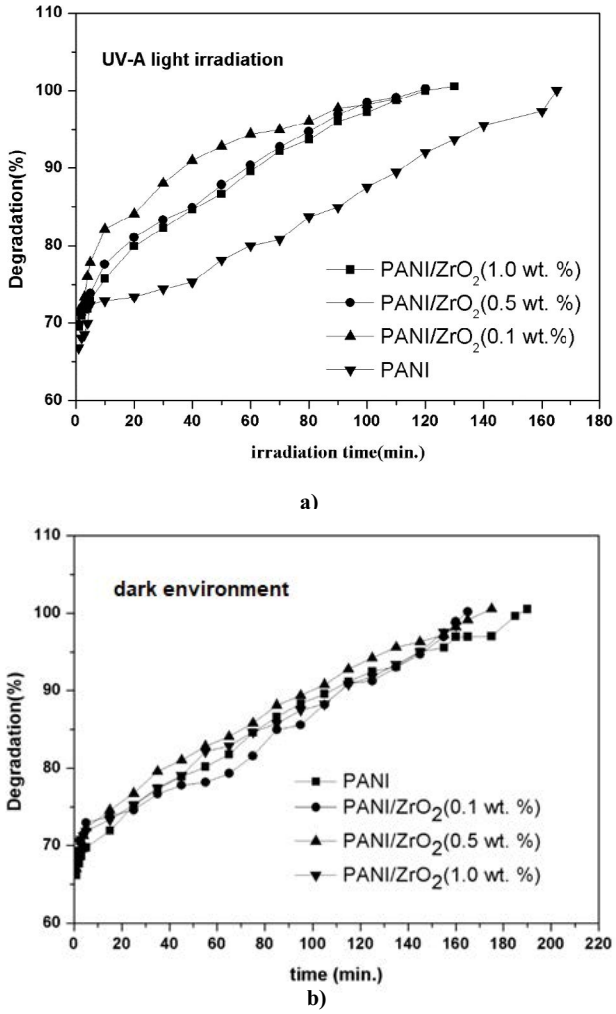

Fig. 8. Degradation (%)-*t* graphs for PANI and PANI/ZrO_2 photocatalysts (a) under UV-A light irradiation and (b) dark environment.

in the polymeric composite, the rate of degradation of the dye was increased and the degradation time decreased (Fig. 8). Under the UV-A light irradiation and darkness medium, photocatalytic activities of 0.1 g PANI and PANI/ZrO_2 were investigated until 100% degradation of the CR dye solution. The 100% degradation time of 100 ppm CR under UV-A light irradiation and dark environment for PANI was 165 and 190 min, respectively. The time to reach 100% degradation in the UV-A light environment for PANI/ZrO_2 (0.1 wt.%) photocatalyst was 130 and 165 min. in the dark environment. As the amount of nanometal (ZrO_2) in the photocatalyst increases, the degradation time in both media decreases. According to this, the photocatalytic activity of photocatalysts increased in UV-A light irradiation compared to the dark environment. Accordingly, it was determined that the adsorption of dye molecules to the catalyst surface was effective in the degradation of dye molecules in the dark environment.

So far in research, ZrO_2 has been reported to be effective only in UV-A light irradiation, and there are not many studies on adsorption capacity in the dark environment. However, if it creates a composite with PANI, it is seen that PANI is also effective in the UV-visible region by providing electron transfer to ZrO_2. Carević et al. [14], the photocatalytic activities of PANI/ZrO_2 nanocomposites were evaluated using photocatalytic degradation reactions and compared with the activity of bare ZrO_2 nanoparticles. Accordingly, the nanocomposites showed improved degradation activities [14,18]. In our study, the degradation of the dye increased as the amount of ZrO_2 in the composite increased, especially under UV-A light irradiation.

3.7. Mechanism of photocatalytic reaction

Photocatalytic degradation is an important pathway for the degradation of pollutants (in the presence of organic contaminants and toxic substances) in the presence of UV light and semiconductor particles. Reactions to the photocatalyst surface can be listed as follows [53–55]:

- Stimulation of photocatalyst by photon absorption,
- Reactant transfer from the liquid phase to the catalyst surface and accordingly adsorption,

- Oxidation and reduction (redox) reactions in the adsorption phase,
- Desorption of products or products resulting from catalysis by photocatalyst surface.

When the semiconductor is irradiated with higher-energy photons than the band-gap energy, electron-hole pairs initiate the chemical reactions in the semiconductors (Eq. (3)). The valence band gaps act as an oxidizer, while the conduction band electrons act as a reducer.

$$ZrO_2 \rightarrow e^-_{iB} + h^+_{VB} \quad (3)$$

The electrons and electron holes in the semiconducting material move to the surface under UV irradiation.

The OH^- ions and H_2O molecules are the most adsorbed substances on the ZrO_2 surface. In both acidic and basic conditions, the OH^- and H_2O groups on the surface undergo oxidation to form $OH^\bullet$ with the valence band spaces of ZrO_2 [54,55]. The formation of $OH^\bullet$ in semiconductors occurs in two forms; by reaction with the H_2O or surface hydroxide groups adsorbed on the valence band holes [Eqs. (4)–(6)].

$$ZrO_2 \rightarrow e^-_{iB} + h^+_{VB} \quad (4)$$

$$h^+_{VB} + H_2O \rightarrow OH^\bullet + H^+ \quad (5)$$

$$h^+_{VB} + OH^- \rightarrow OH^\bullet \quad (6)$$

From $O_2^{\bullet-}$, through H_2O_2 formation, the oxygen that is adsorbed on the surface reacts to give superoxide ions through the conduction band electrons. Under acidic conditions, the per hydroxyl radical ($HO_2^\bullet$) may form from the $O_2^{\bullet-}$ to H^+ reaction. Perhydroxyl radical also causes hydrogen peroxide [Eqs. (7)–(11)].

$$O_2 + e^-_{iB} \rightarrow O_2^{\bullet-} \quad (7)$$

$$O_2^{\bullet-} + H^+ \rightarrow HO_2^\bullet \quad (8)$$

$$HO_2^\bullet + HO_2^\bullet \rightarrow H_2O_2 + O_2 \quad (9)$$

$$O_2^{\bullet-} + HO_2^\bullet \rightarrow HO_2^- + O_2 \quad (10)$$

$$HO_2^- + H^+ \rightarrow H_2O_2 \quad (11)$$

The disintegration of H_2O_2 leads to the $OH^\bullet$ flow. H_2O_2 behaves as an electron acceptor that reduces the recombination of electron-space pairs and induces $OH^\bullet$ [Eqs. (12)–(14)].

$$H_2O_2 + e^-_{iB} \rightarrow OH^\bullet + OH^- \quad (12)$$

$$H_2O_2 + O_2^{\bullet-} \rightarrow OH^\bullet + OH^- + O_2 \quad (13)$$

$$H_2O_2 \rightarrow 2\,OH^\bullet \quad (14)$$

The resulting hydroxyl radicals break down organic impurities into smaller molecules [56]. In addition, holes formed on the surface of the exciting semiconductor act as strongly oxidizing and electrons acting as strong reducing [16,56].

Photocatalytic degradation of the dyes is a complex reaction involving the conversion of the dye to CO_2 and H_2O via a series of intermediates. The mechanism of photocatalytic degradation of CR by using the PANI/ZrO_2 photocatalyst is presented in Fig. 9 [18,57,58].

3.8. Kinetic studies

In general, the photocatalytic degradation of organic molecules on semiconductor metal oxides is determined by the first-order reaction kinetic model [32,43]. The equation

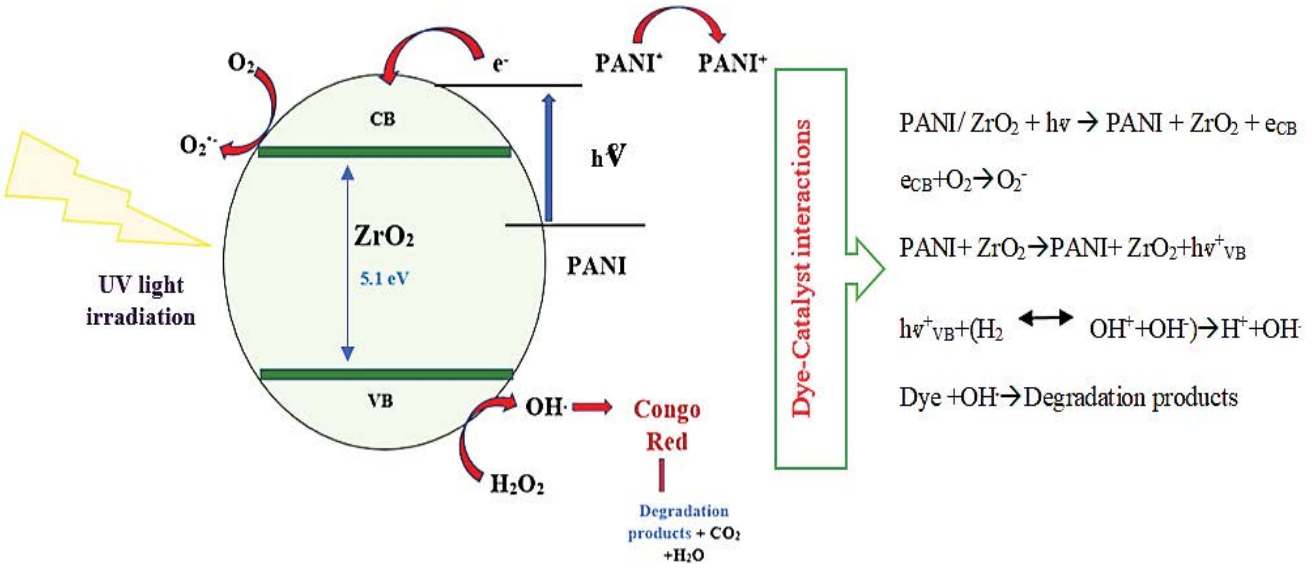

Fig. 9. Schematic representation of photocatalytic degradation reaction mechanism of CR dye.

for the rate constant of photocatalytic decomposition reactions is as follows:

$$\ln\left(\frac{C}{C_0}\right) = -k_t \tag{15}$$

where k is the reaction rate constant or kinetic constant; C_0 is the initial concentration of the dye substance; C is the concentration of the dye after UV irradiation and t is the excitation time.

The $\ln(C/C_0)$-t plots corresponding to the kinetic model of photocatalytic degradation reactions under UV-A light irradiation and darkness are presented in Fig. 10. The first 60 min were taken into consideration for each $\ln(C/C_0)$-t graphs and kinetic studies were performed accordingly.

The reaction rate constants obtained after the backward extrapolation of the $\ln(C/C_0)$-t curves are presented in Table 2. The reaction from the straight lines obtained was adapted to the reaction rate equation from the first order (Fig. 10). Accordingly, as the amount of nano-ZrO_2 (metal oxide) contained in the polymeric nanocomposite increases, the k values increase. This can be explained by the fact that ZrO_2 increases the reaction rate by the catalytic action of the polymeric composite [39].

4. Conclusions

In this study, the chemical polymerization of polyaniline with and without ZrO_2 semiconductor nano-metal oxide particles in different quantities (0.1, 0.5, and 1.0 wt.%) were synthesized and characterized. According to the characterization results (FTIR, XRD, SEM, TEM, and TGA) and UV-visible spectra analysis, it has been determined that ZrO_2 enters the polymeric network structure and increases the thermal stability of the polymer. The photocatalytic degradation of CR was investigated under UV light irradiation and dark environment. The results showed that the photocatalytic effect increased the degradation of the dye in all conditions. This increase has increased due to the increase in the amount of ZrO_2 in the ZrO_2-containing PANI catalyst. The bandgap energy of the ZrO_2 nanoparticle is 4.9 eV and PANI/ZrO_2 nanocomposite is 3.25 eV. The bandgap energy of PANI/ZrO_2 is reduced to 3.25 eV by adding PANI. Also, the kinetic mechanism of the photocatalytic reaction was investigated by the first-order reaction kinetic model. Reaction rate constants were increased by increasing in PANI nano-ZrO_2 amount. As a result of our experimental research, we concluded that this nano-composite can be a preferred material in wastewater treatment due to its simple and economical synthesis methodology and its effect on adsorption and photocatalytic.

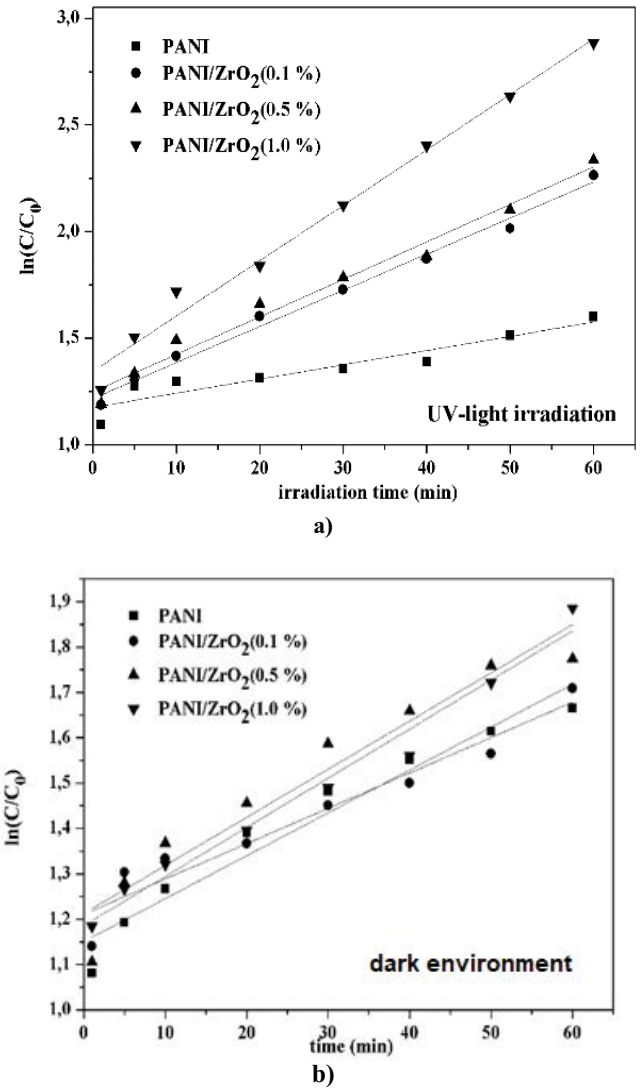

Fig. 10. $\ln(C/C_0)$-t graph for PANI and PANI/ZrO_2 in 100 ppm dye solution (a) UV-A light irradiation and (b) dark environment.

Table 2
Reaction rate constants (k) of CR for PANI and PANI/ZrO_2 under UV-visible light irradiation and dark environment

Polymeric nanocomposites	k (dk^{-1})		R^2	
	UV-visible light	Dark environment	UV-visible light	Dark environment
PANI	0.007	0.006	0.9886	0.9437
PANI/ZrO_2 (0.1 wt.%)	0.16	0.009	0.9778	0.9247
PANI/ZrO_2 (0.5 wt.%)	0.017	0.0106	0.9851	0.9215
PANI/ZrO_2 (1.0 wt.%)	0.025	0.0108	0.8664	0.9762

Acknowledgments

We would like to thank Prof. Dr. Senay Simsek from North Dakota University, who supported XRD, SEM and TEM measurements of characterization of polymeric composites. Also, our study was supported by Kocaeli University Scientific Researches and Project Unit with KOU-BAP 2014/016 project.

References

[1] E.S. Yoo, J. Lıbra, U. Wıesman, Reduction of azo dyes by *Desulfovibrio desulfiricans*, Water Sci. Technol., 14 (2000) 15–22.
[2] P.C. Vandevivere, R. Bianchi, W. Vestreate, Treatment and reuse of wastewater from the textile wet-processing industry: review of emerging technologies, J. Chem. Technol. Biotechnol., 72 (1998) 289–302.
[3] E. Alver, M. Bulut, A.Ü. Metin, H. Çiftçi, One step effective removal of congo red in chitosan nanoparticles by encapsulation, Spectrochim. Acta, Part A, 5 (2017) 132–138.
[4] C. Srilakshmi, R. Saraf, Ag-doped hydroxyapatite as efficient adsorbent for removal of congo red dye from aqueous solution: synthesis, kinetic and equilibrium adsorption isotherm analysis, Microporous Mesoporous Mater., 219 (2016) 134–144.
[5] V.K. Gupta, Suhas, Application of low-cost adsorbents for dye removal–a review, J. Environ. Manage., 90 (2009) 2313–234.
[6] F. Deniz, S. Karaman, Removal of basic red 46 dye from aqueous solution by pine tree leaves, Chem. Eng. J., 170 (2011) 67–74.
[7] L. Yu, Y.-M. Luo, The adsorption mechanism of anionic and cationic dyes by Jerusalem artichoke stalk-based mesoporous activated carbon, J. Environ. Chem. Eng., 2 (2014) 220–229.
[8] A.M. Aljeboree, A.N. Alshirifi, A.F. Alkaim, Kinetics and equilibrium study for the adsorption of textile dyes on coconut shell activated carbon, Arabian J. Chem., 10 (2017) S3381–S3393.
[9] N.M. Mahmoodi, M. Arami, H. Bahrami, S. Khorramfar, Novel biosorbent (*Canola* hull): surface characterization and dye removal ability at different cationic dye concentrations, Desalination, 264 (2010) 134–142.
[10] A. Fujishima, T.N. Rao, D.A. Tryk, TiO_2 photocatalysts and diamond electrodes, Electrochim. Acta, 45 (2000) 4683–4690.
[11] M.R. Hoffmann, S.T. Martin, W. Choi, D.W. Bahnemann, Environmental applications of semiconductor photocatalysis, Chem. Rev., 1 (1995) 69–96.
[12] R. Saravanan, G. Francisco, A. Stephen, Basic Principles, Mechanism, and Challenges of Photocatalysis, Springer Series on Polymer and Composite Materials, Springer, Cham, 2017, pp. 19–40.
[13] S.N. Basahel, T.T. Ali, M. Mokhtar, K. Narasimharao, Influence of crystal structure of nanosized ZrO_2 on photocatalytic degradation of methyl orange, Nanoscale Res. Lett., 18 (2015) 10–73.
[14] M.V. Carević, N.D. Abazović, M.N. Mitrić, G. Ćirić-Marjanović, M.D. Mojović, S.P. Ahrenkiel, M.I. Čomor, Properties of zirconia/polyaniline hybrid nanocomposites and their application as photocatalysts for degradation of model pollutants, Mater. Chem. Phys., 205 (2018) 130–137.
[15] N. Daneshvar, D. Salari, A.R. Khataee, Photocatalytic degradation of azo dye acid red 14 in water: investigation of the effect of operational parameters, J. Photochem. Photobiol., A, 157 (2003) 111–116.
[16] E. Evgenidou, K. Fytianos, I. Poulios, Photocatalytic oxidation of dimethoate in aqueous solutions, J. Photochem. Photobiol., A, 175 (2005) 29–38.
[17] C. Guillard, H. Lachheb, A. Houas, M. Ksibi, E. Elaloui, J.M. Herrmann, Influence of chemical structure of dyes of pH and of inorganic salts on their photocatalytic degradation by TiO_2 comparison of the efficiency of powder and supported TiO_2, J. Photochem. Photobiol., A, 158 (2003) 27–36.
[18] B. Ozbay, N. Genc, İ. Ozbay, B. Baghaki, S. Zor, Photocatalytic activities of polyaniline-modified TiO_2 and ZnO under visible light: an experimental and modeling study, Clean Technol. Environ. Policy, 18 (2016) 2591–2601.
[19] S. Polisetti, A.D. Parag, G. Madras, Photocatalytic activity of combustion synthesized ZrO_2 and ZrO_2–TiO_2 mixed oxides, Ind. Eng. Chem. Res., 50 (2011) 12915–12924.
[20] S.K. Kansal, M. Singh, D. Sud, Studies on photodegradation of two commercial dyes in aqueous phase using different photocatalysts, J. Hazard. Mater., 141(2007) 581–590.
[21] R. Abe, T. Takata, H. Sugihara, K. Domen Photocatalytic overall water splitting under visible light by TaON and WO_3 with an IO_3^-/I^- shuttle redox mediator, Chem. Commun., 30 (2005) 3829–3831.
[22] J. Kim, C.W. Lee, W. Choi, Platinized WO_3 as an environmental photocatalyst that generates OH radicals under visible light, Environ. Sci. Technol., 17 (2010) 6849–6854.
[23] X. Wang, J.C. Yu, Y. Chen, L. Wu, X. Fu, ZrO_2-modified mesoporous nanocrystalline $TiO_{2-x}N_x$ as efficient visible light photocatalysts, Environ. Sci. Technol., 7 (2006) 2369–2374.
[24] R. Thiruvenkatachari, S. Vigneswaran, I.S. Moon, A review on UV/TiO_2 photocatalytic oxidation process, Korean J. Chem. Eng., 1 (2008) 64–72.
[25] F. Falbe, M. Regnitz, Chemilexikon, 9.Auflage, George Thieme Verlag, Stutgart, 1992.
[26] S.A. Nabi, M. Shahadat, R. Bushra, M. Oves, F. Ahmed, Synthesis and characterization of polyaniline Zr(IV) sulphosalicylate composite and its applications (1) electrical conductivity, and (2) antimicrobial activity studies, Chem. Eng. J., 173 (2011) 706–714.
[27] I. Azocar, E. Vargas, N. Duran, A. Arrieta, E. Gonzalez, J. Pavez, M.J. Kogan, J.H. Zagal, M.A. Paez, Preparation and antibacterial properties of hybrid-zirconia films with silver nanoparticles, Mater. Chem. Phys., 137 (2012) 396–403.
[28] H. Zhu, S. Peng, W. Jiang, Electrochemical properties of PANI as single electrode of electrochemical capacitors in acid electrolytes, Sci. World J., 2013 (2013) 1–8.
[29] A. Tiselius, S. Hjerten, O. Levin, Protein chromatography on calcium phosphate columns, Arch. Biochem. Biophys., 65 (1956) 132–55.
[30] K. Zare, H. Sadegh, R. Shahryari-ghoshekandi, B. Maazinejad, V. Ali, S. Agarwal, V.K. Gupta, Enhanced removal of toxic congo red dye using multi walled carbon nanotubes: kinetic, equilibrium studies and its comparison with other adsorbents, J. Mol. Liq., 212 (2015) 266–271.
[31] A. Riede, M. Helmstedt, V. Riede, J. Stejskal, In situ polymerized polyaniline films. 2. Dispersion polymerization of aniline in the presence of colloidal silica, J. Am. Chem. Soc., 15 (2002) 6240–6244.
[32] Q.X. Zhang, Z.Z. Yu, X.L. Xie, Y.W. Mai, Crystallization and impact energy of polypropylene/$CaCO_3$ nanocomposites with nonionic modifier, Polymer, 17 (2004) 5985–5994.
[33] D.F. Skoog, T. Nieman, E. Kılıç, F. Köseoğlu, H. Yılmaz, Eds., Enstrümantal Analiz Kitabı (Instrumental Analysis Book), 5th ed, Ankara, Bilim Yayıncılık, 1992.
[34] W. Zheng, M. Angelopoulos, A.J. Epstein, A.G. Mc Diarmid, Concentration dependence of aggregation of polyaniline in NMP solution and properties of resulting cast films, Macromolecules, 30 (1997) 2953–2955.
[35] S.G. Pawar, S.L. Patil, M.A. Chougule, A.T. Mane, D.M. Jundale, V.B. Patil, Synthesis and characterization of polyaniline: TiO_2 nanocomposites, Int. J. Polym. Mat. Polym. Biomater., 59 (2010) 777–785.
[36] T. Anwer, M.O. Ansari, F. Mohammad, Dodecyl benzene sulfonic acid micelles assisted in situ preparation and enhanced thermoelectric performance of semiconducting polyaniline–zirconium oxide nanocomposites, J. Ind. Eng. Chem., 19 (2013) 1653–1658.
[37] S. Sultana, Rafiuddin, M.Z. Khan, K. Umar, Synthesis and characterization of copper ferrite nanoparticles doped polyaniline, J. Alloys Compd., 535 (2012) 44–49.
[38] A.A. Farghali, M. Moussa, M.H. Khedr, Synthesis and characterization of novel conductive and magnetic nano-composites, J. Alloys Compd., 499 (2010) 98–103.
[39] S. Sultana, Rafiuddin, M.Z. Khan, K. Umar, M. Muneer, Electrical, thermal, photocatalytic and antibacterial studies of

metallic oxide nanocomposite doped polyaniline, J. Mater. Sci. Technol., 9 (2013) 795–800.
[40] F.C. Masim-Wu, C.H. Tsai, Y.F. Lin, M.L. Fu, M. Liu, F. Kang, Y.F. Wang, Synergistic effect of PANI-ZrO_2 composite as antibacterial, anti-corrosion, and phosphate adsorbent material: synthesis, characterization and applications, Environ. Technol., 40 (2017) 1–13.
[41] H.M. Altass, S.K. Abd El Rahman, Surface and catalytic properties of triflic acid supported zirconia: effect of zirconia tetragonal phase, J. Mol. Catal. A: Chem., 411 (2016) 138–145.
[42] B.P. Prasanna, D.N. Avadhani, H.B. Muralidhara, K. Chaitra, V.R. Thomas, M. Revanasiddappa, N. Kathyayini, Synthesis of polyaniline/ZrO_2 nanocomposites and their performance in AC conductivity and electrochemical supercapacitance, Bull. Mater. Sci., 39 (2016) 667–675.
[43] J.P. Pouget, C.H. Hsu, A.G. Mac Diarmid, A.J. Epstein, Structural investigation of metallic PAN-CSA and some of its derivatives, Synth. Met., 69 (1995) 119–120.
[44] H. Huang, Z.C. Guo, W. Zhu, F.C. Li, Preparation and characterization of conductive polyaniline/zirconia nanoparticles composites, Adv. Mater. Res., 221 (2011) 302–307.
[45] K. Gopalakrishnan, C. Ramesh, M. Elango, M. Thamilselvan, Optical and magnetic studies on Cu_2O/PANI nanocomposite prepared by chemical polymerization method, ISRN Mat. Sci., 2014 (2014) 1–7.
[46] D.Y. Godovsky, A.E. Varfolomeev, D.F. Zaretsky, R.L.N. Chandrakanthi, A. Kündig, C. Weder, W. Caseri, Preparation of nanocomposites of polyaniline and inorganic semiconductors, J. Mater Chem., 11 (2001) 2465–2469.
[47] M.D.A. Khan, J. Akhtar, M.A. Malik, M. Akhtar, N. Revaprasadu, Phase-pure fabrication and shape evolution studies of SnS nanosheets, New J. Chem., 39 (2015) 9569.
[48] H.Q. Cao, X.Q. Qiu, B. Luo, Y. Liang, Y.H. Zhang, R.Q. Tan, M.J. Zhao, Q.M. Zhu, Synthesis and room-temperature ultraviolet photoluminescence properties of zirconia nanowires, Adv. Funct. Mater., 3 (2004) 243–246.
[49] S. Verma, S. Rani, S. Kumar, Tetragonal zirconia quantum dots in silica matrix prepared by a modified sol–gel protocol, Appl. Phys. A, 124 (2018) 387.
[50] G.K. Sidhu, N. Kumar, R. Kumar, Study the structural and optical behaviour of polyaniline/ZrO_2 nanocomposites, AIP Conf. Proc., 1953 (2018) 030220.
[51] S. Patnaik, K. Kumar Das, A. Mohanty, K. Parida, Enhanced photo catalytic reduction of Cr(VI) over polymer-sensitized g-C_3N_4/$ZnFe_2O_4$ and its synergism with phenol oxidation under visible light irradiation, Catal. Today, 315 (2018) 52–66.
[52] S. Vijayalakshmi, E. Kumar, P.S. Venkatesh, A. Raja, Preparation of zirconium oxide with polyaniline nanocatalyst for the decomposition of pharmaceutical industrial wastewater, Ionics, 26 (2020) 1507–1513.
[53] D.B. Hamal, K.J. Klabunde, Synthesis, characterization, and visible light activity of new nanoparticle photocatalysts based on silver, carbon, and sulfur-doped TiO_2, J. Colloid Interface Sci., 311(2007) 514–522.
[54] K.I. Konstantinou, A.A. Triantafyllos, TiO_2-assisted photocatalytic degradation of azo dyes in aqueous solution: kinetic and mechanistic investigations: a review, Appl. Catal., B, 49 (2004) 1–14.
[55] C.S. Turchi, D.F. Ollis, Photocatalytic degradation of organic water contaminants: mechanism involving hydroxyl radical attack, J. Catal., 122 (1990) 178–192.
[56] C. Shifu, L. Yunzhang, Study on the photocatalytic degradation of glyphosate by TiO_2 Photocatalyst, Chemosphere, 67 (2007) 1010–1017.
[57] E. Evgenidou, I. Konstantinou, K. Fytianos, I. Poulios, T. Albanis, Photocatalytic oxidation of methyl parathion over TiO_2 and ZnO suspensions, Catal. Today, 124 (2007) 156–162.
[58] A.A. Shah, S. Akhlaq, M. Sayed, S. Bilal, N. Ali, Synthesis and characterization of polyaniline–zirconium dioxide and polyaniline–cerium dioxide composites with enhanced photocatalytic degradation of rhodamine B dye, Chem. Pap., 72 (2018) 2523–2538.